On the Quantification of Boundary Layer Effects on Flame Temperature Measurements Using Line-of-sight Absorption Spectroscopy

Liuhao Ma, Kin-Pang Cheong, Min Yang, Chaokai Yuan & Wei Ren

Taylor & Francis
Taylor & Francis Group

Check for updates

On the Quantification of Boundary Layer Effects on Flame Temperature Measurements Using Line-of-sight Absorption Spectroscopy

Liuhao Ma[a], Kin-Pang Cheong[b], Min Yang[a], Chaokai Yuan[c], and Wei Ren [ID][a]

[a]Department of Mechanical and Automation Engineering, Shenzhen Research Institute, the Chinese University of Hong Kong, Hong Kong SAR, China; [b]School of Aeronautics and Astronautics, Sichuan University, Chengdu, Sichuan, China; [c]State Key Laboratory of High Temperature Gas Dynamics, Institute of Mechanics, Chinese Academy of Sciences, Beijing, China

ABSTRACT

We studied the boundary layer effects on flame temperature measurements using line-of-sight (LOS) absorption spectroscopy. The primary objective is to quantify the measurement uncertainty of the LOS-determined temperature, which is influenced by the thermal and species boundary layers existing in standard laminar premixed flames. The boundary layer thickness (δ), central flame temperature (T_c) and species concentration (X_c) are the major factors investigated in this work. Typical absorption lines of H_2O in the wavelength range of 1.4–2.9 μm were examined under different boundary layer conditions (δ/L = 0–50%, L is the optical path length above the flame; T_c = 1400–2200 K; and X_c = 14–20%). As a result, the thermal boundary layer is observed to contribute mainly to the temperature deviation of the LOS measurement, which increases with δ and T_c. In comparison, the variation of X_c between 14% and 20% has a negligible effect on the temperature measurement in the presence of both thermal and species boundary layers. A systematical investigation of all the selected line pairs reveals that a properly selected line pair reduces the temperature deviation by a maximum of 16.8% under typical laminar flame conditions. The particular line pair centered at 4029.52 cm^{-1} and 4030.73 cm^{-1}, which could be detected by a single tunable semiconductor laser, is recommended for the LOS temperature measurement over a temperature range of 1400–2200 K. Finally, we performed a case study of five representative temperature measurements in laminar flames and successfully corrected the LOS-determined temperature by taking into account the boundary layer effects.

Introduction

Laser diagnostics have been rapidly developed and extensively used in the past decade for combustion research due to their non-intrusiveness and superior spatio-temporal resolution (Goldenstein et al. 2017). The representative laser-based techniques for combustion include Raman scattering (Cantu et al. 2018), laser-induced fluorescence (Zhou et al. 2015), absorption and dispersion spectroscopy (Ma et al. 2018a, 2019), laser-induced

incandescence (Chatterjee and Gülder 2018), and laser-induced breakdown spectroscopy (Letty et al. 2010). Among these optical techniques, laser absorption spectroscopy (LAS) represents one of the most widely-used methods owing to its fast, sensitive and quantitative measurement with a relatively simple optical configuration (Hanson 2011; Liu and Xu 2019).

As a typical line-of-sight (LOS) measurement, LAS is readily applicable to the uniform flow field where temperature, species concentration, pressure and velocity are constant along the optical path. However, such an ideal flow does not exist in actual combustion environments due to the influence of boundary layers. When sensing reactive flows with non-negligible thermochemical gradients, the LOS measurement is potentially prone to a large measurement uncertainty (Zhou et al. 2003). Therefore, the effects of non-uniformity on LOS measurements and the methods to alleviate these effects have been explored for a long term by the combustion community.

In the previous studies, the boundary layer has been identified as a major region that affects the accuracy of LOS measurement, even when the boundary layer is very thin compared to the main flow (Liu 2006). Zhou et al. (2003) observed a temperature deviation of ~140 K for LOS flame measurements caused by the boundary layer effect. Liu et al. (2005) experimentally investigated the non-uniform temperature distribution by evaluating different absorption line pairs and discovered the hot thermal boundary layer near the combustor walls. Schoenung and Hanson (1980) proposed the concept of *effective* absorption path with the assistance of probe measurements to correct the boundary layer effect on absolute species concentration measurements in flames.

The methods of multi-line thermometry (Liu, Jeffries, Hanson 2007; Ma, Lau, Ren 2017; Sanders et al. 2001; Zhang et al. 2016) and tomographic reconstruction (Cheong et al. 2019; Liu et al. 2018; Nau et al. 2015; Wei et al. 2018; Xia et al. 2017) were often used to characterize the thermochemical distribution within the boundary layer. However, more complex signal and data processing algorithms are required in these methods. Hence, researchers also spent numerous efforts in minimizing the influence of boundary layers so that the LOS measurement is still representative for the central flame temperature. Wagner et al. (2012) explored the method of using absorption lines that are insensitive to the temperature gradient region for species concentration measurements in laminar counter-flow diffusion flames. Goldenstein et al. (2013) used two absorption transitions with linear temperature-dependent line-strengths to reduce the evident discrepancy between the path-integrated and the path-averaged absorption profiles in the presence of thermochemical boundary layers. Sepman et al. (2017) exploited transitions with the modest temperature dependence to minimize the boundary layer effects on temperature measurements in a biomass gasifier.

Although the boundary layer effect has been identified as an important factor affecting LOS measurements, very few studies have been performed to quantify the influence of boundary layers, particularly on the LOS-determined temperature and species concentration. Recently Qu, Werhahn, and Ebert (2018) quantified the thermal boundary layer effect on CO_2 concentration measurements in a two-zone high-temperature gas cell by taking into account the temperature gradient effect.

As temperature is very important for understanding the physicochemical process in fundamental combustion studies, the primary objective of this work is to provide a systematic and quantitative investigation of boundary layer effects on temperature

measurements in standard laminar premixed flames. The axisymmetric laminar flame (i.e., McKenna burner) normally contains a uniform hot-core region and a boundary layer with thermochemical gradient. Based on the two-line absorption thermometry of H_2O, nine commonly used line pairs in the spectral range between 1.4 μm and 2.9 μm are selected for investigation. The boundary layer effects caused by both the mere thermal boundary layer and the combined thermal and species boundary layer are investigated under different flame conditions. A semi-empirical approach to obtain a more accurate central flame temperature is also proposed in this study.

Spectroscopic fundamentals

Here we briefly describe the spectroscopic fundamentals of LAS. The basic equation governing the LOS absorption measurement is the Beer-Lambert relation (Hanson, Spearrin, Goldenstein 2016):

$$\left(\frac{I_t}{I_0}\right)_v = \exp(-k_v L) = \exp\left(-\int_0^L P(x)S_i(T(x))X_{abs}(x)\phi_v dx\right) \tag{1}$$

where I_0 and I_t are the incident and transmitted laser intensities at the optical frequency v, respectively; k_v [cm^{-1}] is the spectral absorption coefficient contributed from all the adjacent absorption transitions, L [cm] is the total path length, and the product $k_v \cdot L$ is known as the spectral absorbance; x is the position along the optical path; $S_i(T)$ [cm^{-2} atm^{-1}] is the line-strength of the specific transition i which is only a function of gas temperature T [K], φ_v [cm] is the line-shape function, P [atm] is the total gas pressure, X_{abs} is concentration of the absorbing species. The temperature-dependent line-strength is given by:

$$S(T) = S(T_0)\frac{Q(T_0)}{Q(T)}\left(\frac{T_0}{T}\right)\exp\left[-\frac{hcE''}{k}\left(\frac{1}{T}-\frac{1}{T_0}\right)\right]\left[1-\exp\left(-\frac{hcv_0}{kT}\right)\right]\left[1-\exp\left(-\frac{hcv_0}{kT_0}\right)\right]^{-1} \tag{2}$$

where the partition function $Q(T)$ and line-strength $S(T_0)$ can be found in the HITRAN database (Gordon et al. 2017). As the line-shape function φ_v is normalized such that its integral over the entire frequency range is unity, the spectrally integrated absorbance A_i (also known as the integrated area) can be expressed as:

$$A_i = \int_{-\infty}^{\infty} k_v L dv = \int_0^L P(x)S_i(T(x))X_{abs}(x)dx \tag{3}$$

According to the two-line thermometry, temperature can be inferred from the ratio of the integrated absorbances of two absorption lines using the following equation:

$$T = \frac{\frac{hc}{k}(E_2'' - E_1'')}{\ln(\frac{A_1}{A_2}) + \ln(\frac{S_2(T_0)}{S_1(T_0)}) + \frac{hc}{k}\frac{(E_2''-E_1'')}{T_0}} \tag{4}$$

where h [J·s] is Planck's constant, c [cm·s^{-1}] is the light speed, k [J·K^{-1}] is the Boltzmann constant, v_0 is the line-center frequency, and E'' represents the lower state energy of the transition.

Methodology

Boundary layer effect

For laminar flames stabilized on a porous media or honeycomb structure, significant thermal and species concentration boundary layers exist near the flame edge. According to the previous studies (Guha and Schoegl 2014; Liu et al. 2015; Ma et al. 2020; Yu et al. 2010), both temperature and H_2O concentrations along the LOS remain constant in the central region and then decreases gradually to the ambient condition. The thermal boundary layer and the H_2O concentration boundary layer have almost the identical thickness. Figure 1(a) demonstrates the representative distributions of temperature and H_2O concentration in a CH_4/air premixed flame at the equivalence ratio Φ = 0.95 and pressure P = 1.0 atm. The central porous media of the burner has a diameter of 60 mm indicated by the blue shaded area in Figure 1(a). The gray shaded regions indicate the boundary layers. The thermal boundary layer thickness, δ_T, is defined as the distance from the location at room temperature to that at 99% of the central flame temperature (T_c). The species boundary layer thickness, δ_{H2O}, is defined in a similar way.

Based on the boundary layer conditions shown in Figure 1(a), the simulated absorption spectra of H_2O near 2.5 μm are illustrated in Figure 1(b). The detailed values of the simulated peak absorbance and integrated area under different boundary layer conditions are summarized in Table S1 of the Supplementary Material. The presence of boundary layers affects the peak absorbances of both lines (4029.52 cm^{-1} and 4030.73 cm^{-1}) particularly for the line centered at 4029.52 cm^{-1} due to its smaller E''. For instance, the absorption line at 4029.52 cm^{-1} with a smaller E'' is more sensitive to the cold boundary layer and thus its absorbance is affected more evidently by the temperature variation along the optical
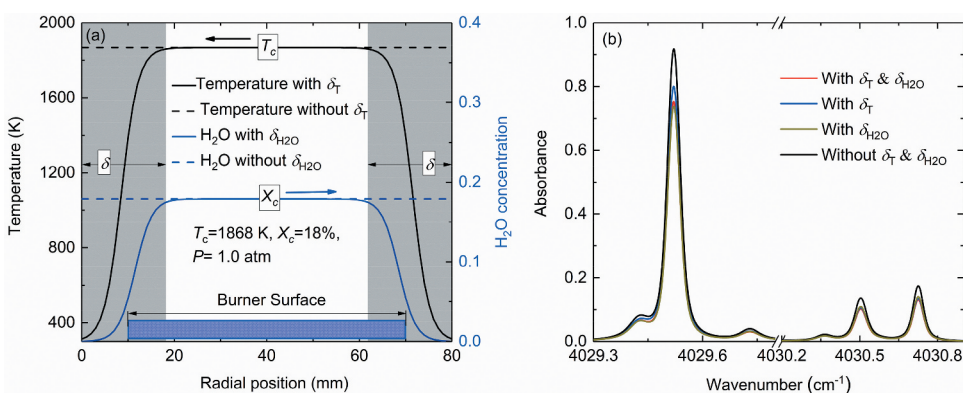

Figure 1. (a) Representative radial distributions of temperature and H_2O concentration (gray shaded area, boundary layer; blue shaded area, central porous media; dashed line, uniform flame condition). (b) Simulated absorption lines of H_2O at 4029.52 and 4030.73 cm^{-1} under different boundary layer conditions (δ_T/L and δ_{H2O}/L are both set to be 45.4%).

path. As temperature is inferred from the ratio of the integrated absorbances shown in Eqn. (4), it is interesting to observe that the ratio of the two integrated areas remains unchanged when there is only a concentration boundary layer. Hence, the mere concentration boundary layer has no influence on the temperature measurement. Therefore, in this study we only explore the effects of the thermal boundary layer and the combined thermal/concentration boundary layer.

Line-pair selection

The line-selection criteria for two-line thermometry have been well documented elsewhere (Liu 2006; Zhou et al. 2003). In general, the selected absorption lines should have a good spectral isolation from nearby transitions and interfering species, a large absorption line-strength and a high temperature sensitivity. Several additional selection rules have also been proposed to reduce the boundary layer effect and improve the precision (Goldenstein et al. 2013).

Here we study all the line pairs of H_2O that have been used for temperature sensing in combustion environments (Farooq, Jeffries, Hanson 2008; Goldenstein et al. 2013, 2015; Lee et al. 2020; Li, Farooq, Hanson 2011; Liu et al. 2015; Ma et al. 2020, 2018b; Peng et al. 2019, 2016; Peng, Strand, Hanson 2020; Qu et al. 2015; Wang et al. 2020, 2015; Wu et al. 2017; Zeng et al. 2018; Zhou et al. 2003). These line pairs cover the wavelength range from 1 μm to 3 μm as illustrated in Figure 2(a), belonging to the overtone ($2\nu_3$), combination ($\nu_1+\nu_3$, $\nu_2+\nu_3$), and fundamental (ν_3) bands. The spectroscopic parameters of these H_2O lines are listed in Table 1; and these parameters are taken either from the HITRAN database (Gordon et al. 2017) or from the validation experiments (Farooq, Jeffries, Hanson 2008; Goldenstein 2014; Li, Farooq, Hanson 2011; Liu 2006; Zhou 2005). Among these H_2O lines, the line pairs numbering 6–9 at 1.4 μm and 1.8 μm ($2\nu_3$, $\nu_1+\nu_3$, $\nu_2+\nu_3$) have been used for flame and engine measurements by employing telecommunication fiber-coupled diode lasers (Goldenstein et al. 2015; Lee et al. 2020; Peng, Strand, Hanson 2020; Qu et al. 2015; Wang et al. 2020, 2015; Wu et al. 2017; Zeng et al. 2018). The other line pairs numbering 1–5 at 2.5–2.9 μm (ν_3) are receiving more attention recently due to their stronger line-strengths and have been used for laboratory-scale flames (Farooq, Jeffries, Hanson 2008; Li, Farooq, Hanson 2011; Ma et al. 2018b; Peng et al. 2016) and practical propulsion engines (Peng et al. 2019). Figure 2(b) compares the temperature sensitivity of these line pairs. Although line pairs 5, 8, 9 have a low temperature sensitivity at 2000–3000 K, we still involve them for investigation considering their frequent applications in combustion diagnostics. The temperature sensitivity is defined as the derivative of Equation (4) with respect to temperature:

$$\left|\frac{dR/R}{dT/T}\right| \approx \left(\frac{hc}{k}\right)\frac{\left|E_2^{''} - E_1^{''}\right|}{T} \tag{5}$$

Simulation of temperature deviation

We aim to quantify the deviation of LOS-determined temperature measured under different boundary layer conditions, which are specified by the boundary layer thickness (δ), the central flame temperature (T_c), and the species concentration (X_c). The absolute
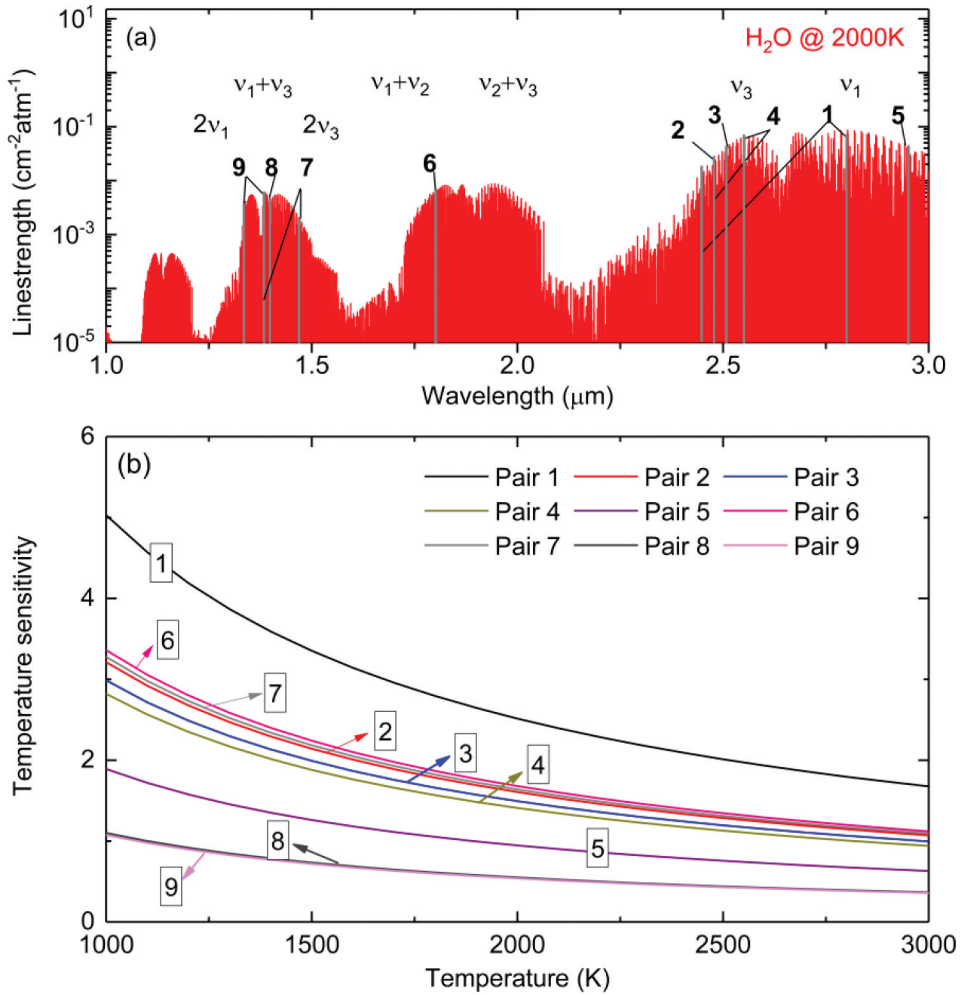
Figure 2. (a) Representative line pairs of H_2O previously used for temperature measurements. (b) Comparison of temperature sensitivity for the selected line pairs at 1000–3000 K.

temperature deviation ($\Delta T = T_c - T_{LOS}$) is defined as the difference between the LOS-determined temperature (T_{LOS}) and the actual central temperature T_c. Additionally, we define the relative temperature deviation (ε) as the ratio of ΔT and T_c.

Figure 3 presents the flowchart of numerically evaluating the temperature deviation caused by the boundary layer effects. The input parameters include those describing the thermochemical and boundary layer conditions (e.g., T_c, T_{edge}, X_c, X_{edge}, δ, k_{slope}), the laser wavelength range covering the target spectral features, and the spectroscopic parameters. The LOS absorption spectra of the selected absorption transitions are simulated under different flame conditions. The integrated absorbance is obtained by fitting the absorption profiles using the multi-Voigt function and Levenberg-Marquardt (L-M) algorithm. The temperature deviation is ultimately determined by the difference of the derived temperature T_{LOS} and the central temperature T_c.

Table 1. Spectroscopic parameters of the representative line pairs.

Line pair #	Frequency (cm^{-1})	Wavelength (nm)	S @296 K (cm^{-2}atm^{-1})	E″ (cm^{-1})	ΔE″ (cm^{-1})
1[a]	4083.89	2448.65	3.00×10^{-8}	4331.07	3488.71
	3565.67	2804.52	3.36×10^{-1}	842.36	
2[b]	4030.73	2480.94	2.68×10^{-9}	4889.49	2228.54
	4029.52	2481.69	1.10×10^{-4}	2660.95	
3[b]	3982.75	2510.83	5.92×10^{-7}	3654.04	2072.71
	3982.06	2511.26	9.13×10^{-3}	1581.33	
4[b]	4029.52	2481.69	1.10×10^{-4}	2660.95	1956.75
	3920.08	2550.97	6.35×10^{-1}	704.20	
5[b]	3459.73	2890.41	5.14×10^{-6}	3386.00	1312.50
	3460.59	2889.68	3.32×10^{-3}	2073.50	
6[b]	5553.86	1800.57	7.55×10^{-7}	3314.86	2331.95
	5554.18	1800.45	7.80×10^{-3}	982.91	
7[b]	6806.03	1469.29	6.40×10^{-7}	3291.15	2246.09
	7185.60	1391.67	1.96×10^{-2}	1045.06	
8[a]	7153.74	1397.87	8.59×10^{-6}	2552.86	763.82
	7154.35	1397.75	3.68×10^{-4}	1789.04	
9[b]	7444.35/7444.37	1343.30	1.12×10^{-3}	1774.75/1806.67	745.65
	7185.60	1391.67	1.96×10^{-2}	1045.06	

[a]HITRAN 2016 database (Gordon et al. 2017);
[b]Validated in experiments (Farooq, Jeffries, Hanson 2008; Goldenstein 2014; Li, Farooq, Hanson 2011; Liu 2006; Zhou 2005).
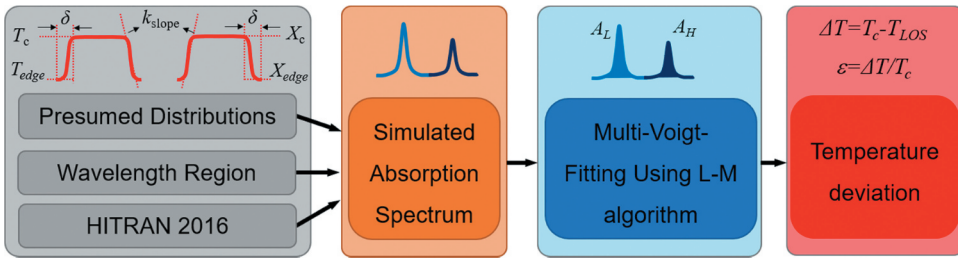
Figure 3. Flowchart of numerically evaluating the boundary layer effect on LOS-determined temperature.

To simulate the non-uniform environment, the optical path is normally discretized into numerous elements, each of which is assumed to have a uniform thermochemical property. Here an elemental length of 0.1 mm is used in the simulation for the total optical path length of 80 mm. The finer discretization has a negligible influence on the calculation result, which can be seen from Fig. S1 of the Supplementary Material. The central flame temperature investigated in this study ranges from 1400 K to 2200 K, which covers most laminar flame experiments. The representative results of the simulated absorption spectra along with the Voigt-fitting profiles are provided in Fig. S2 of the Supplementary Material.

Results and discussion

Effect of thermal boundary layer

As the integrated absorbance is mainly dependent on temperature, the effect of the thermal boundary layer is firstly explored before considering both thermal and concentration boundary layers to be discussed in Section 4.2. In this section we discuss the variation of temperature deviation (ΔT) with the thickness of thermal boundary layer (δ_T) and the
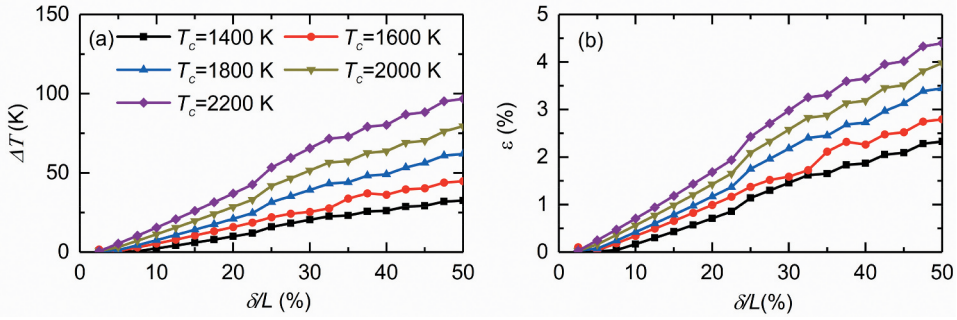
Figure 4. Variation of LOS-determined temperature with boundary layer thickness for different values of T_c: (a) absolute deviation (ΔT), (b) relative deviation (ε).

central flame temperature (T_c). First, we take the line pair 2 with the largest E" as an example to interpret the simulation results. Figure 4 plots the variation of the absolute (ΔT) and relative (ε) deviations of temperature with the boundary layer thickness. It is evident that the LOS-determined temperature deviates further from T_c with the increased δ. A deviation of ~ 100 K (or ~4.4%) is observed at the highest temperature of 2200 K. At the fixed δ, the deviation (either ΔT or ε) increases with the central flame temperature T_c.

To better view the thermal boundary effect, we summarize the results of all the selected line pairs in a contour plot illustrated in Figure 5. The deviation always has a positive value for all the line pairs, indicating that the LOS-determined temperature is consistently lower than T_c. At an arbitrary T_c between 1400 K and 2200 K, the deviation increases with the boundary layer thickness. Due to the different sensitivities to the thermal boundary layer, all these selected line pairs demonstrate very different results of temperature deviations. For instance, line pairs 7 and 8 have the largest deviation over 10% as shown in Figure 5; but line pairs 2, 3 and 5 show a deviation mostly below 6% even for a very large boundary layer thickness ($\delta/L = 50\%$). This is mainly because these three line pairs have a larger E'' ($E_s'' > 1581.33$ cm^{-1}, $E_L'' > 3386.00$ cm^{-1}). Particularly, line pair 2 shows the best immunity to the effect of thermal boundary layer over the entire temperature range and under different boundary layer conditions.

It is of interest to find out the boundary layer condition, corresponding to a very small temperature deviation, so that the LOS measurement is still valid. Here we define a critical boundary layer thickness ($\delta_{critical}$), which leads to a ε-value of 2% or less. Such a $\delta_{critical}$ at different temperatures could be readily identified in Figure 5 for line pairs 2–5, 8 and 9. Hence, the accuracy of the LOS temperature measurement is acceptable when the critical condition of boundary layer satisfies. A good example is the temperature measurement above a long flat burner (Farooq, Jeffries, Hanson 2008), which has a narrow non-uniform flame region ($\delta/L < 4\%$). The LOS-determined temperature using line pair 3 was in an excellent agreement with the thermocouple result (Farooq, Jeffries, Hanson 2008).

It is known that the boundary layer mainly influences the integrated area of absorbance due to the varied line-strength along the absorption path. Here we take line pair 4 as an example to quantify the effect of boundary layer thickness on the temperature deviation. Figure 6(a) plots the temperature-dependent line-strengths of the two absorption lines centered at 4029.52 cm^{-1} and 3920.08 cm^{-1}, respectively. The corresponding line-strength
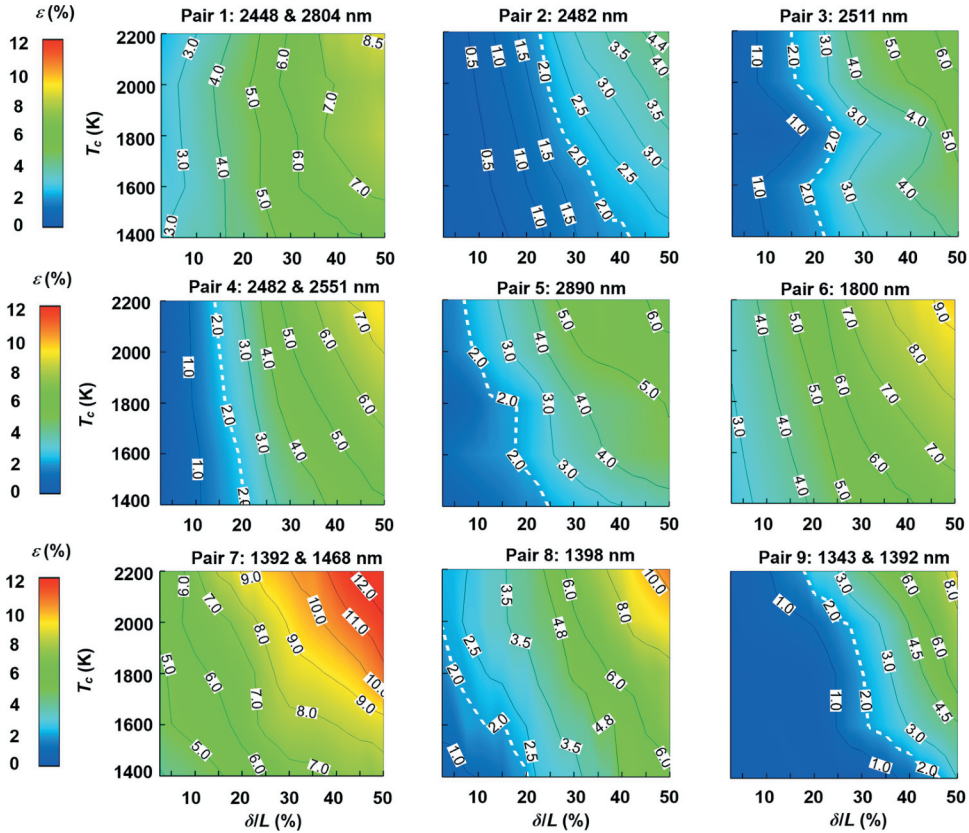
Figure 5. Contour of the temperature deviation (ε) caused by the thermal boundary layer for all the 9 line pairs listed in Table 1.

distributions along the absorption path are plotted in Figure 6(b,c), respectively, for a central flame temperature of 2200 K and ambient temperature of 300 K. Three different boundary layer conditions (δ/L = 10%, 20% and 50%) are investigated for comparison. Note that the total optical path ($2L$) is fixed while the boundary layer thickness (2δ) varies. Figure 6(b) shows that the absorption line with a smaller E'' (denoted as E_s'') has a larger line-strength within the boundary layer than that in the central flame, leading to a larger integrated area of absorbance A_s. In comparison, the other line with a larger E'' (denoted as E_L'') undergoes an initial increase of the line-strength followed by a decline from the central flame to the edge. As a result, an overall decrease in the integrated area A_L of absorbance is obtained as illustrated in Figure 6(c). Hence, the ratio of these two integrated areas increases due to the existence of the thermal boundary layer, which under-estimates the central flame temperature. A similar line-strength plot for line pair 2 is illustrated in Fig. S3 of the Supplementary Material.

Combined thermal and concentration boundary layer

The concentration boundary layer always accompanies with the thermal boundary layer. Hence, the combined effects of thermal and concentration boundary layers are investigated
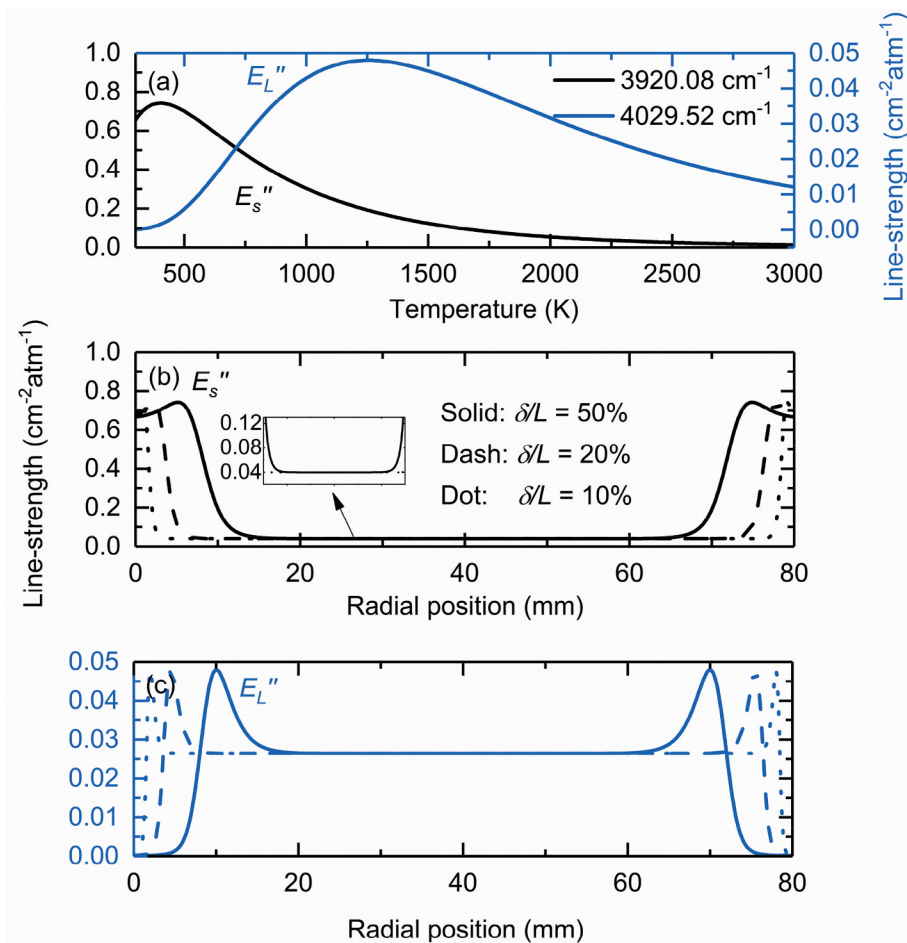
Figure 6. (a) Temperature-dependent line-strengths of the two absorption lines in line pair 4. (b) Radial distribution of line-strength of the absorption line with a smaller E_s''. (c) Radial distribution of line-strength of the absorption line with a larger E_L''. Flame condition: $T_c = 2200$ K; $\delta/L = 10\%$, 20% and 50%, respectively.

in terms of δ, T_c and X_c. As discussed in Section 3.1, the thickness of the concentration boundary layer is treated the same as that of the thermal boundary layer.

Figure 7 illustrates the contour plots of temperature deviation for all the line pairs by varying δ and T_c. The temperature deviation increases gradually with δ over the entire temperature range. The largest deviation appears at the top-right corner of the contour plot for each line pair, corresponding to the flame with the highest central temperature and the largest boundary layer thickness. In particular, the maximum ε ranges from 4.8% for line pair 2 to 21.6% for pair 7 under the condition of $\delta/L = 50\%$ and $T_c = 2200$ K. By comparing the results to Figure 5, the additional concentration boundary layer increases the temperature deviation of most line pairs except the line pairs 2 and 8. It is of interest to observe that the combined thermal/concentration boundary layers for line pairs 2 and 8 have almost the identical effect to that caused by the mere thermal boundary layer. These two line-pairs have
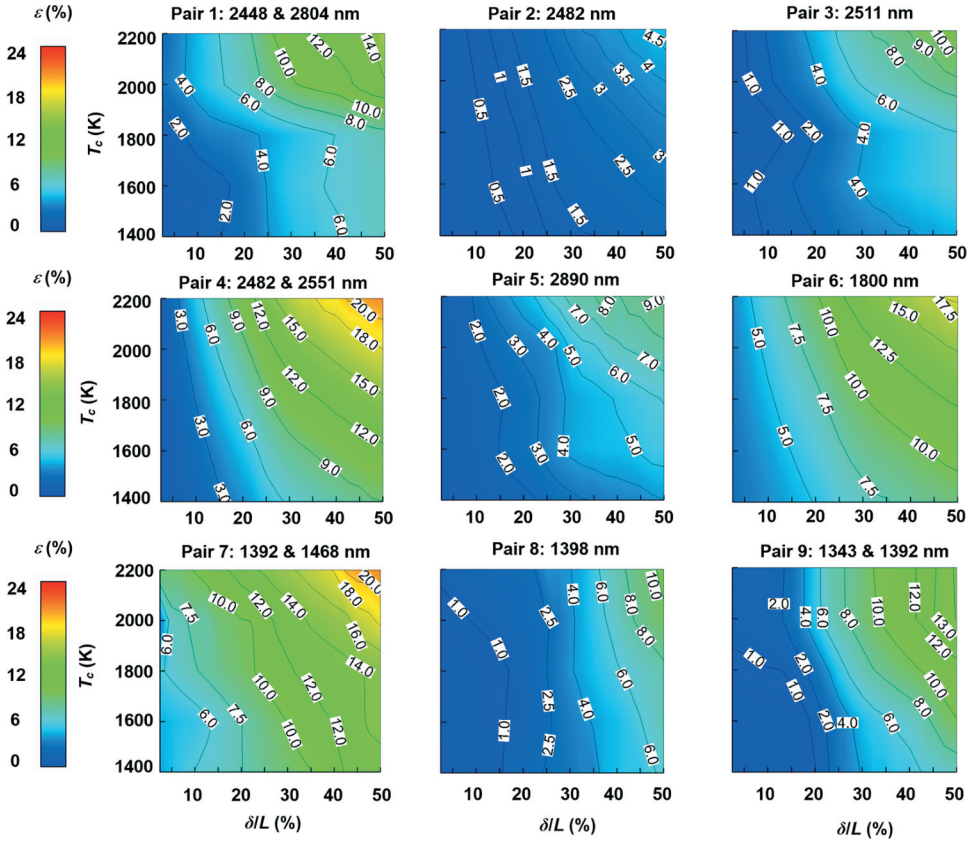
Figure 7. Contour of temperature deviation (ε) caused by the combined temperature and concentration boundary layers for all the 9 line pairs.

much smaller line-strengths at low temperatures, making them insensitive to the concentration variation in the cold boundary layer.

The variation of the central gas composition may also affect the inferred temperature, which is investigated under different flame conditions. Figure 8 presents the simulation results of three line pairs 2, 4, and 6 as an example. For the typical CH_4/air laminar premixed flames with $\Phi = 0.7-1.2$, the H_2O concentration is known to be in the range of 15%–19%; and the H_2O concentration is much lower for the other hydrocarbon/air (e.g., C_2H_4, C_3H_8) flames or the flames with N_2/CO_2 dilutions. Therefore, the H_2O concentration is varied over a wide range from 14% to 20% for investigation. Although the integrated absorbance of the individual absorption line varies with the gas composition, the calculated temperature deviation is almost irrelevant to the variation of the gas composition as illustrated in Figure 8.

Case study in flame measurement

Our numerical analysis reveals that the LOS-determined temperature is lower than the actual temperature of the central flame by an amount of ΔT. Here case studies of the
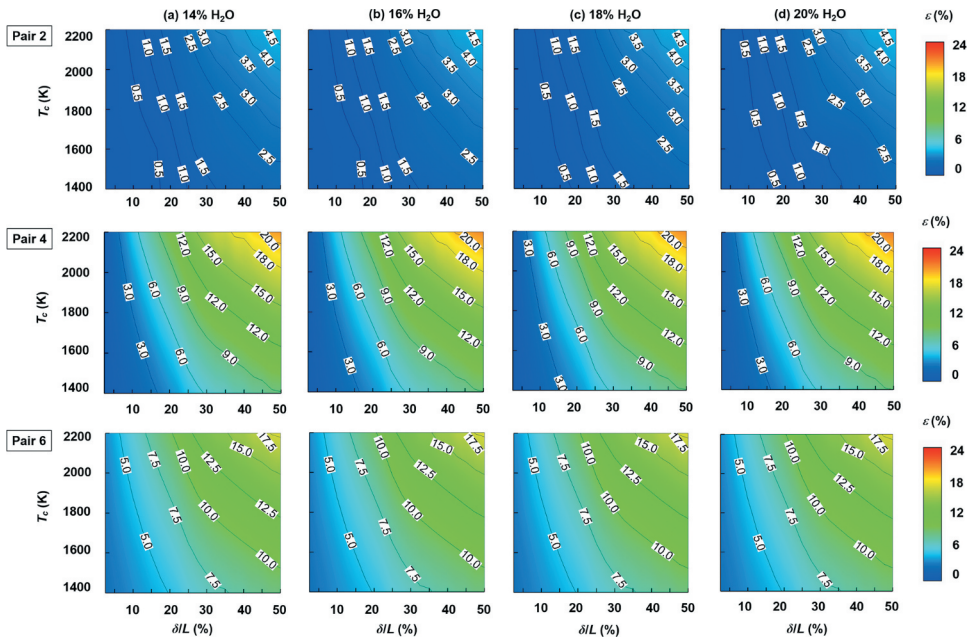
Figure 8. Contour of temperature deviation caused by the combined temperature and concentration boundary layers for line pairs 2, 4 and 6. The H_2O concentration at the central flame is varied between 14% and 20% for investigation.

Table 2. Experimental details of the five representative laser absorption measurements.

	Case 1[This work]	Case 2[This work]	Case 3[(Zhou et al. 2003)]	Case 4[(Fu et al. 2020)]	Case 5[This work]
Line pair	2	4	6	8	9
Reactants	CH_4/air	CH_4/air	C_2H_4/air	CH_4/air	CH_4/air
Equivalence ratio	0.8–1.2	0.8–1.2	0.65	0.85–1.22	0.8–1.2
Burner type	McKenna	McKenna	Hencken	McKenna	McKenna
Co-flow	Nitrogen	Nitrogen	NA	NA	Nitrogen
HAB	5 mm	5 mm	10 mm	6 mm	5 mm

previous LOS flame measurements are performed based on the conclusions made in this work.

The experimental conditions are summarized in Table 2. For the McKenna burner, measurements were performed at the height above the burner (HAB) of 5–6 mm. For the Hencken burner, measurements were taken at the HAB of 10 mm. For the CH_4/air flames studied in cases 1, 2 and 5, the equivalence ratio was varied between 0.8 and 1.2 by changing the air flow rate but fixing the CH_4 flow rate at 1.5 L/min. The optical setup is almost identical to the recent study described in (Ma et al., 2018b), which is also provided in Fig. S4 of the Supplementary Material. The reference central flame temperature was obtained using the thermocouple, the LAS profile-fitting method, and the CFD simulation (Ma et al. 2020). For case 3, the flow rates of C_2H_4 and air were set to be 2.9 L/min and 64 L/min, respectively, to obtain an equivalence ratio of 0.65 (Zhou et al. 2003); and the central flame temperature

was measured by the thermocouple and the profile-fitting method (Zhou et al. 2003). For case 4, the varied equivalence ratios (Φ = 0.85–1.22) were obtained by changing the CH_4 flow rate while fixing the air flow rate at 14.5 L/min (Fu et al. 2020). The CFD simulation was performed using the recent numerical framework (Ma et al. 2020) and the simulated central flame temperature was used as the reference. With the knowledge of boundary layer thickness and the reference central temperature, the temperature deviations can be determined. In general, such information can be obtained using an easily accessible thermocouple, a low-cost infrared CCD camera (pyrometry), or even the CFD simulation. For the laminar flame investigated in the current work, we used the results from the previous experiments (e.g., thermocouple measurement) and the CFD simulations (Fu et al. 2020; Ma et al. 2020; Zhou et al. 2003). The flame conditions for the above cases are added to the corresponding temperature deviation contours shown in Figure 9. For each of the case listed in Table 2, the temperature deviations of all the measurements fall into the shaded region in Figure 9. Although cases 1 and 4 have a relatively small deviation (1.5–2.7% and 2.7–5%, respectively), the other cases (cases 2, 3, and 5) have a very large deviation of 6–12% which could not be accepted for temperature determination.

Figure 10 presents the original LOS-determined temperature without correction, the reference T_c, and the corrected LOS-determined temperature for each case. The overall temperature can be obtained by adding the correction determined from Figure 9 to the original LOS measurement. As illustrated in Figure 10(a), the original LOS-determined temperature was consistently lower than the reference T_c. For cases 1, 2 and 5 (equivalence ratio Φ = 1.0), the boundary layer thickness was evaluated to be 12 mm (δ/L = 30%) based on the experimental measurement using the thermocouple measurement and CFD simulation. The relative temperature deviations were determined to be 1.7% (case 1), 12% (case 2) and 7.8% (case 5), respectively, according to the boundary layer effects shown in Figure 9. The overall corrected LOS-determined temperature is in good agreement with the reference values mostly within a difference of 1.2%; the maximum difference between the corrected LOS-determined temperature and the reference temperature is 3.6% at Φ = 0.8 for case 5.

For case study 3, with the temperature deviation of 155 K considered as shown in Fig. 11, the LOS-determined temperature was corrected to be 1775 K, showing a good agreement with the thermocouple measurement (1740 K) and the LAS profile-fitting result (1760 K). Similarly, the LOS-determined temperature for case 4 is always below the reference temperature when Φ is changed from 0.85 to 1.23. The corrected LOS-determined temperature agrees well with the CFD simulation within a relative difference of 1.0%.
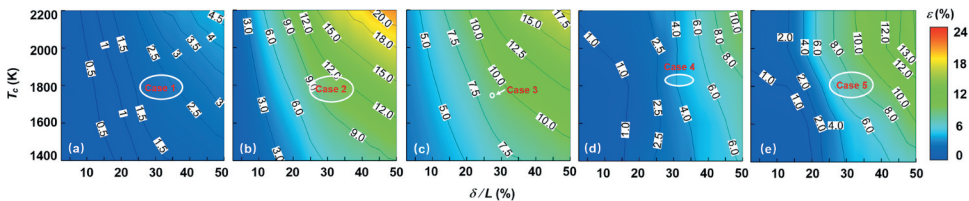

Figure 9. Temperature deviations of the investigated cases: (a) case 1, (b) case 2, (c) case 3, (d) case 4, and (e) case 5.
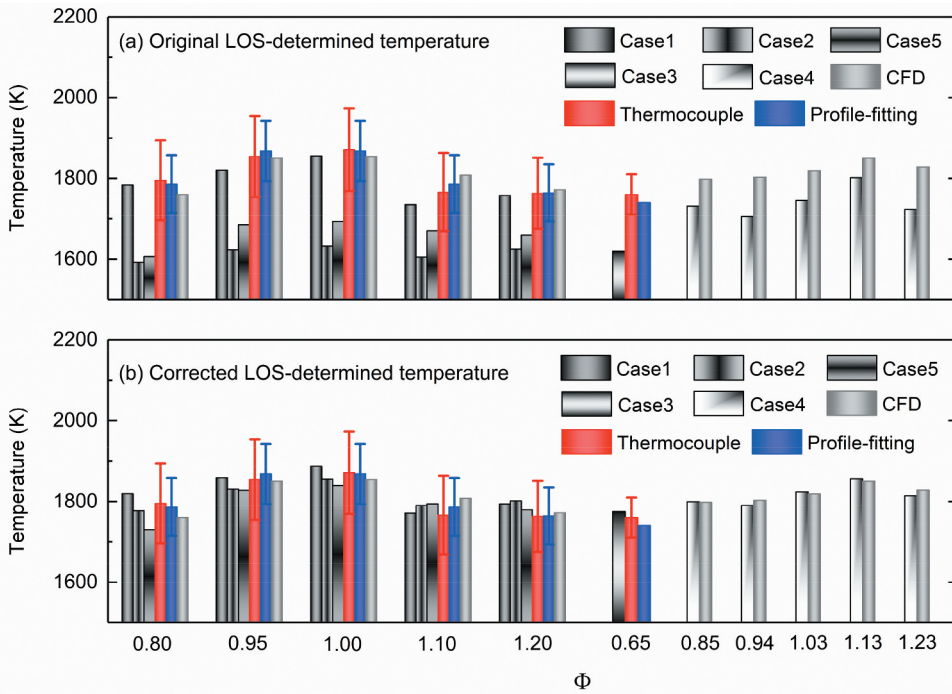
Figure 10. (a) Comparison of the original LOS-determined temperature and the reference central flame temperature. (b) Comparison of the corrected LOS-determined temperature and the reference central flame temperature for the five representative cases listed in Table 2.

Conclusions

We performed a quantitative investigation of the boundary layer effects on temperature measurements using LOS absorption spectroscopy in laminar premixed flames. The temperature deviation between the LOS-determined temperature and the actual central flame temperature was evaluated by considering the thermal and concentration boundary layers. As a demonstration, we studied a total of nine line pairs of H_2O that have been widely used for temperature sensing in combustion environments. Compared with the species concentration boundary layer, the thermal boundary layer has a more significant influence on the LOS-determined temperature. The temperature deviation increases gradually with δ and T_c over the entire temperature range of 1400–2200 K. The additional species concentration boundary layer increases the temperature deviation for most line pairs. However, the temperature deviations are irrelevant to the variation of X_c between 14% and 20% in the presence of both thermal and species concentration boundary layers. Among all the line pairs investigated in this study, the largest temperature deviation of 21.6% is expected for a boundary layer thickness of $\delta/L = 50\%$ and central flame temperature of 2200 K. The line pair of 4029.52 cm^{-1} and 4030.73 cm^{-1} is recommended for the LOS temperature measurement at 1400–2200 K due to its good immunity to boundary layer effects. As a general rule to further reduce the measurement uncertainty, we suggest the selection of line pairs with larger $E^{''}$, larger difference of $E^{''}$, smaller line-strength at low temperature and larger line-strength at high temperature. By performing the case studies of flame measurements, the LOS-

determined temperature could be corrected by taking into account the boundary layer effects. We expect this work to be valuable for a better design of two-line thermometry and a more accurate interpretation of the experimental data obtained in flame studies.

Nomenclature

k_v	Gas absorption coefficient at frequency v (cm^{-1})
I_0	Incident light intensity
I_t	Transmitted light intensity
$S_i(T)$	Line-strength (cm^{-2} atm^{-1}) of the specific transition i
$S_i(T_0)$	Line-strength at a reference temperature T_0 (296 K)
φ_v	line-shape function (cm)
P	Total gas pressure (atm)
X_{abs}	Absorbing gas species concentration
L	Optical path length (cm)
A_i	Integrated absorbance (cm^{-1}) of the specific transition i
h	Planck's constant (J s)
c	Light speed (cm/s)
k	Boltzmann constant (J/K)
E''	Lower state energy (cm^{-1})
$\Delta E''$	Difference of lower state energy (cm^{-1})
$Q(T)$	Partition function at temperature T
$Q(T_0)$	Partition function at a reference temperature T_0 (296 K)
T_c	Central flame temperature (K)
X_c	Central species concentration
ΔT	Absolute temperature deviation (K)
ε	Relative temperature deviation (%)
δ	Boundary layer thickness
$\delta_{critical}$	Critical boundary layer thickness
δ_T	Thermal boundary layer thickness
δ_{H2O}	Boundary layer thickness of H_2O concentration profile
T_{edge}	Temperature near the flame edge
X_{edge}	Species concentration near the flame edge

ORCID

Wei Ren 🄳 http://orcid.org/0000-0001-6681-593X

References

Cantu, L. M., J. Grohmann, W. Meier, and M. Aigner. 2018. Temperature measurements in confined swirling spray flames by vibrational coherent anti-stokes Raman spectroscopy. *Exp. Therm. Fluid Sci.* 95:52–59. doi:10.1016/j.expthermflusci.2018.01.029.

Chatterjee, S., and Ö. L. Gülder. 2018. Soot concentration and primary particle size in swirl-stabilized non-premixed turbulent flames of ethylene and air. *Exp. Therm. Fluid Sci.* 95:73–80. doi:10.1016/j. expthermflusci.2018.01.035.

Cheong, K.-P., L. Ma, Z. Wang, and W. Ren. 2019. Influence of line pair selection on flame tomography using infrared absorption spectroscopy. *Appl. Spectrosc.* 73 (5):529–39. doi:10.1177/ 0003702818815181.

Farooq, A., J. B. Jeffries, and R. K. Hanson. 2008. In situ combustion measurements of H_2O and temperature near 2.5 μm using tunable diode laser absorption. . *Measurement Science and Technology* 19 (7):075604. doi:10.1088/0957-0233/19/7/075604.

Fu, P., L. Hou, Z. Wang, and X. Chao 2020. Multi-parameters measurements in kerosene-fuelled combustion using tunable diode laser absorption spectroscopy, China National Symposium on Combustion, Xiamen, China.

Goldenstein, C. S. 2014. Wavelength-modulation spectroscopy for determination of gas properties in hostile environments, Ph.D Dissertation, Stanford University.

Goldenstein, C. S., I. A. Schultz, J. B. Jeffries, and R. K. Hanson. 2013. Two-color absorption spectroscopy strategy for measuring the column density and path average temperature of the absorbing species in nonuniform gases. *Appl. Opt.* 52 (33):7950–62. doi:10.1364/ AO.52.007950.

Goldenstein, C. S., R. M. Spearrin, J. B. Jeffries, and R. K. Hanson. 2015. Infrared laser absorption sensors for multiple performance parameters in a detonation combustor. *Proc. Combust. Inst.* 35 (3):3739–47. doi:10.1016/j.proci.2014.05.027.

Goldenstein, C. S., R. M. Spearrin, J. B. Jeffries, and R. K. Hanson. 2017. Infrared laser-absorption sensing for combustion gases. *Prog. Energy Combust. Sci.* 60:132–76. doi:10.1016/j. pecs.2016.12.002.

Gordon, I., L. Rothman, C. Hill, R. Kochanov, Y. Tan, P. Bernath, M. Birk, V. Boudon, A. Campargue, and K. Chance. 2017. The HITRAN2016 molecular spectroscopic database. *J. Quant. Spectrosc. Radiat. Transf.* 203:3–69. doi:10.1016/j.jqsrt.2017.06.038.

Guha, A., and I. Schoegl. 2014. Tomographic laser absorption spectroscopy using Tikhonov regularization. *Appl. Opt.* 53 (34):8095–103. doi:10.1364/AO.53.008095.

Hanson, R. K. 2011. Applications of quantitative laser sensors to kinetics, propulsion and practical energy systems. *Proc. Combust. Inst.* 33 (1):1–40. doi:10.1016/j.proci.2010.09.007.

Hanson, R. K., R. M. Spearrin, and C. S. Goldenstein. 2016. *Spectroscopy and optical diagnostics for gases.* Switzerland: Springer.

Lee, J., C. Bong, J. Yoo, and M. S. Bak. 2020. Combined use of TDLAS and LIBS for reconstruction of temperature and concentration fields. *Optics Express* 28 (14):21121–33. doi:10.1364/OE.396909.

Letty, C., A. Pastore, E. Mastorakos, R. Balachandran, and S. Couris. 2010. Comparison of electrical and laser spark emission spectroscopy for fuel concentration measurements. *Experimental Thermal and Fluid Science* 34 (3):338–45. doi:10.1016/j.expthermflusci.2009.10.018.

Li, S., A. Farooq, and R. K. Hanson. 2011. H_2O temperature sensor for low-pressure flames using tunable diode laser absorption near 2.9 μm. *Measurement Science and Technology* 22 (12):125301. doi:10.1088/0957-0233/22/12/125301.

Liu, C., and L. Xu. 2019. Laser absorption spectroscopy for combustion diagnosis in reactive flows: A review. *Appl. Spectrosc. Rev.* 54 (1):1–44. doi:10.1080/05704928.2018.1448854.

Liu, C., L. Xu, F. Li, Z. Cao, S. A. Tsekenis, and H. McCann. 2015. Resolution-doubled one-dimensional wavelength modulation spectroscopy tomography for flame flatness validation of a flat-flame burner. *Applied Physics B* 120 (3):407–16. doi:10.1007/s00340-015-6150-9.

Liu, J. T., G. B. Rieker, J. B. Jeffries, M. R. Gruber, C. D. Carter, T. Mathur, and R. K. Hanson. 2005. Near-infrared diode laser absorption diagnostic for temperature and water vapor in a scramjet combustor. *Appl. Opt.* 44 (31):6701–11. doi:10.1364/AO.44.006701.

Liu, X. 2006. Line-of-sight absorption of H_2O vapour: Gas temperature sensing in uniform and nonuniform flows. Ph.D Dissertation, Stanford University.

Liu, X., G. Zhang, Y. Huang, Y. Wang, and F. Qi. 2018. Two-dimensional temperature and carbon dioxide concentration profiles in atmospheric laminar diffusion flames measured by mid-infrared

direct absorption spectroscopy at 4.2 μm. *Applied Physics B* 124 (4):61. doi:10.1007/s00340-018-6930-0.

Liu, X., J. B. Jeffries, and R. K. Hanson. 2007. Measurement of non-uniform temperature distributions using line-of-sight absorption spectroscopy. *AIAA J.* 45 (2):411–19. doi:10.2514/1.26708.

Ma, L., H. Ning, J. Wu, K.-P. Cheong, and W. Ren. 2018a. Characterization of temperature and soot volume fraction in laminar premixed flames: Laser absorption/extinction measurement and two-dimensional computational fluid dynamics modeling. *Energy & Fuels* 32 (12):12962–70. doi:10.1021/acs.energyfuels.8b03111.

Ma, L., H. Ning, J. Wu, and W. Ren. 2018b. In situ flame temperature measurements using a mid-infrared two-line H_2O laser-absorption thermometry. *Combustion Science and Technology* 190 (3):393–408. doi:10.1080/00102202.2017.1392515.

Ma, L., K.-P. Cheong, H. Ning, and W. Ren. 2020. An improved study of the uniformity of laminar premixed flames using laser absorption spectroscopy and CFD simulation. *Exp. Therm. Fluid Sci.* 110013. doi:10.1016/j.expthermflusci.2019.110013.

Ma, L., Z. Wang, K.-P. Cheong, H. Ning, and W. Ren. 2019. Mid-infrared heterodyne phase-sensitive dispersion spectroscopy in flame measurements. *Proc. Combust. Inst.* 37 (2):1329–36. doi:10.1016/j.proci.2018.06.184.

Ma, L. H., L. Y. Lau, and W. Ren. 2017. Non-uniform temperature and species concentration measurements in a laminar flame using multi-band infrared absorption spectroscopy. *Applied Physics B* 123 (3):83. doi:10.1007/s00340-017-6645-7.

Nau, P., J. Koppmann, A. Lackner, K. Kohse-Höinghaus, and A. Brockhinke. 2015. Quantum cascade laser-based MIR spectrometer for the determination of CO and CO_2 concentrations and temperature in flames. *Appl. Phy. B.* 118 (3):361–68. doi:10.1007/s00340-014-5992-x.

Peng, W. Y., C. L. Strand, and R. K. Hanson. 2020. Analysis of laser absorption gas sensors employing scanned-wavelength modulation spectroscopy with 1f-phase detection. *Applied Physics B* 126 (1):1–23. doi:10.1007/s00340-019-7369-7.

Peng, W. Y., C. S. Goldenstein, R. M. Spearrin, J. B. Jeffries, and R. K. Hanson. 2016. Single-ended mid-infrared laser-absorption sensor for simultaneous in situ measurements of H_2O, CO_2, CO, and temperature in combustion flows. *Appl. Opt.* 55 (33):9347–59. doi:10.1364/AO.55.009347.

Peng, W. Y., S. J. Cassady, C. L. Strand, C. S. Goldenstein, R. M. Spearrin, C. M. Brophy, J. B. Jeffries, and R. K. Hanson. 2019. Single-ended mid-infrared laser-absorption sensor for time-resolved measurements of water concentration and temperature within the annulus of a rotating detonation engine. *Proc. Combust. Inst.* 37 (2):1435–43. doi:10.1016/j.proci.2018.05.021.

Qu, Z., O. Werhahn, and V. Ebert. 2018. Thermal boundary layer effects on line-of-sight tunable diode laser absorption spectroscopy (TDLAS) gas concentration measurements. *Appl. Spectrosc.* 72 (6):853–62. doi:10.1177/0003702817752112.

Qu, Z., R. Ghorbani, D. Valiev, and F. M. Schmidt. 2015. Calibration-free scanned wavelength modulation spectroscopy – Application to H_2O and temperature sensing in flames. *Optics Express* 23 (12):16492–99. doi:10.1364/OE.23.016492.

Sanders, S. T., J. Wang, J. B. Jeffries, and R. K. Hanson. 2001. Diode-laser absorption sensor for line-of-sight gas temperature distributions. *Appl. Opt.* 40 (24):4404–15. doi:10.1364/AO.40.004404.

Schoenung, M., and R. K. Hanson. 1980. CO and temperature measurements in a flat flame by laser ab orption spectroscopy and probe techniques. . *Combustion Science and Technology* 24 (5–6):227–37. doi:10.1080/00102208008952442.

Sepman, A., Y. Ögren, Z. Qu, H. Wiinikka, and F. M. Schmidt. 2017. Real-time in situ multi-parameter TDLAS sensing in the reactor core of an entrained-flow biomass gasifier. *Proc. Combust. Inst.* 36 (3):4541–48. doi:10.1016/j.proci.2016.07.011.

Wagner, S., M. Klein, T. Kathrotia, U. Riedel, T. Kissel, A. Dreizler, and V. Ebert. 2012. Absolute, spatially resolved, in situ CO profiles in atmospheric laminar counter-flow diffusion flames using 2.3 μm TDLAS. *Appl. Phy. B.* 109 (3):533–40. doi:10.1007/s00340-012-5242-z.

Wang, F., Q. Wu, Q. Huang, H. Zhang, J. Yan, and K. Cen. 2015. Simultaneous measurement of 2-dimensional H_2O concentration and temperature distribution in premixed methane/air flame using TDLAS-based tomography technology. *Opt. Commun.* 346:53–63. doi:10.1016/j.optcom.2015.02.015.

Wang, Z., P. Fu, L. Hou, and X. Chao. 2020. Diffuse-reflection-based single-ended laser absorption sensor for H$_2$O temperature and concentration in kerosene-fuelled combustor. *Measurement Science and Technology* 31 (10):105202. doi:10.1088/1361-6501/ab803b.

Wei, C., D. I. Pineda, L. Paxton, F. N. Egolfopoulos, and R. M. Spearrin. 2018. Mid-infrared laser absorption tomography for quantitative 2D thermochemistry measurements in premixed jet flames. *Applied Physics B* 124 (6):123. doi:10.1007/s00340-018-6984-z.

Wu, Q., F. Wang, M. Li, J. Yan, and K. Cen. 2017. Simultaneous in-situ measurement of soot volume fraction, H$_2$O concentration, and temperature in an ethylene/air premixed flame using tunable diode laser absorption spectroscopy. *Combustion Science and Technology* 189 (9):1571–90. doi:10.1080/00102202.2017.1308358.

Xia, H., R. Kan, Z. Xu, Y. He, J. Liu, B. Chen, C. Yang, L. Yao, M. Wei, and G. Zhang. 2017. Two-step tomographic reconstructions of temperature and species concentration in a flame based on laser absorption measurements with a rotation platform. *Optics and Lasers in Engineering* 90:10–18. doi:10.1016/j.optlaseng.2016.09.005.

Yu, X., F. Li, L. Chen, and X. Zhang. 2010. Spatial resolved temperature measurement based on absorption spectroscopy using a single tunable diode laser. *Acta Mechanica Sinica* 26 (1):147–49. doi:10.1007/s10409-009-0296-9.

Zeng, H., F. Li, X. Yu, D. Ou, and L. Chen. 2018. Measurement of multispecies concentration and gas temperature in an ammonium-dinitramide-based thruster by tunable diode lasers. *Appl. Opt.* 57 (6):1321–30. doi:10.1364/AO.57.001321.

Zhang, G., J. Liu, Z. Xu, Y. He, and R. Kan. 2016. Characterization of temperature non-uniformity over a premixed CH$_4$–air flame based on line-of-sight TDLAS. *Applied Physics B* 122 (1):3. doi:10.1007/s00340-015-6289-4.

Zhou, B., C. Brackmann, Q. Li, Z. Wang, P. Petersson, Z. Li, M. Aldén, and X.-S. Bai. 2015. Distributed reactions in highly turbulent premixed methane/air flames: Part I. Flame structure characterization. *Combustion and Flame* 162 (7):2937–53. doi:10.1016/j.combustflame.2014.12.021.

Zhou, X. 2005, Diode-laser absorption sensors for combustion control, Ph.D Dissertation, Stanford University.

Zhou, X., X. Liu, J. B. Jeffries, and R. K. Hanson. 2003. Development of a sensor for temperature and water concentration in combustion gases using a single tunable diode laser. *Measurement Science and Technology* 14 (8):1459–68. doi:10.1088/0957-0233/14/8/335